

# Dream-to-Recon: Monocular 3D Reconstruction with Diffusion-Depth Distillation from Single Images

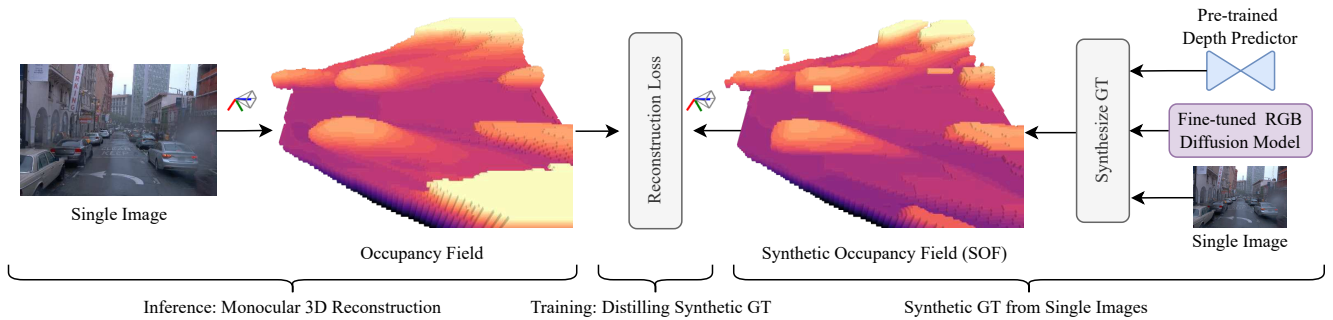
Philipp Wulff<sup>1</sup>Felix Wimbauer<sup>1,2</sup>Dominik Muhle<sup>1,2,3</sup>Daniel Cremers<sup>1,2</sup><sup>1</sup>Technical University of Munich <sup>2</sup>MCML <sup>3</sup>SE3 Labs[philippwulff.github.io/dream-to-recon](https://philippwulff.github.io/dream-to-recon)

Figure 1. **Dream-to-Recon.** We leverage fine-tuned diffusion models for inpainting and a pre-trained depth predictor to generate high-quality scene geometry from a single image, as seen on the right side. Afterwards, we distill a feed-forward scene reconstruction model, which performs on par with reconstruction methods trained with multi-view supervision. The color in the plots indicates the up-coordinate.

## Abstract

*Volumetric scene reconstruction from a single image is crucial for a broad range of applications like autonomous driving and robotics. Recent volumetric reconstruction methods achieve impressive results, but generally require expensive 3D ground truth or multi-view supervision. We propose to leverage pre-trained 2D diffusion models and depth prediction models to generate synthetic scene geometry from a single image. This can then be used to distill a feed-forward scene reconstruction model. Our experiments on the challenging KITTI-360 and Waymo datasets demonstrate that our method matches or outperforms state-of-the-art baselines that use multi-view supervision, and offers unique advantages, for example regarding dynamic scenes. For more details and code, please check out our [project page](#).*

## 1. Introduction

Understanding the 3D geometry of a scene from a single image is fundamental for a wide range of applications, in particular for autonomous driving and robotics. A dense reconstruction of the environment enables machines to react to their surroundings and to reason about further actions such as path planning.

Traditionally, this task has been mainly approached via monocular depth estimation (MDE), where a network predicts per-pixel distance values for a given single image. Through architectural improvements, scaled-up datasets with high-quality ground-truth, and cross-dataset training, these methods have achieved strong generalization capabilities and can be used in an off-the-shelf way [1, 38, 44, 65]. In particular, MDE methods are now even able to predict metric-scale depth maps. While MDE is already useful for many applications, it has a severe limitation: Depth maps are only a 2D projection of the 3D scene, and do not capture the scene’s full 3D structure. Consequently, it is not possible to infer information about areas that are beyond the parts visible in the input image. This limitation makes pure MDE unsuitable for many 3D understanding tasks, e.g. planning the path of a vehicle into a parking spot that was only partially observed.

To address this shortcoming, a new line of work aims to infer a *volumetric 3D reconstruction* of the scene from a single image [4, 27, 28, 37, 53, 60]. Here, the 3D geometry is either represented as a discrete voxel grid [4, 28, 53] or as a continuous density field [27, 37, 60]. Many approaches are trained in a fully-supervised way using dense 3D annotations. However, such 3D ground truth is difficult and expensive to obtain, e.g. by accumulating Lidar scans from a

moving vehicle over time. Even then, dynamic scenes with many moving objects pose a significant challenge, as accumulation over time can lead to trailing artifacts and inconsistencies. Recent works propose to avoid the need for explicit 3D ground-truth from Lidar by using a self-supervised loss based on multi-view consistency and volume rendering [22, 27, 37, 60]. Notably, Behind the Scenes (BTS) [60] demonstrates accurate volumetric reconstruction, even in occluded areas, by relying on multi-view image data captured from a moving car. Despite its impressive performance, BTS still requires a special multi-camera setup and accumulation of views over time to have sufficient observations of the scene. Furthermore, this training scheme is still not robust towards dynamic objects.

Recently, there has also been impressive progress in the field of scene generation, enabled by the success of image diffusion models. Several works combine image diffusion models with pre-trained depth predictors to generate novel views of a scene using the *render-refine-repeat* framework [7, 17, 29]. Starting from an input image, they first warp the pixels into a virtual novel view using the depth predictor. Then, they inpaint and refine the warped image using an image diffusion model, which is conditioned on the warped pixels. By repeating this process multiple times, it is possible to generate several consistent views of a 3D environment and subsequently optimize a 3D representation such as 3D Gaussian Splatting. So far, these methods have focused on generating high-fidelity novel views of constrained scenes. However, the generated geometry, which is important for many downstream tasks, is still lacking in quality. Furthermore, these approaches are very compute-intensive and not (yet) suitable for real-time applications.

In this work, we propose a specialized approach based on the *render-refine-repeat* framework to generate high-quality geometry reconstructions of a scene from a single image. Given a color image and its predicted depth, we render novel views, jointly remove artifacts and inpaint occluded regions. Subsequently, we fuse all views into a 3D occupancy field. These generated scene geometries are then distilled into a robust feed-forward model for single-image volumetric 3D reconstruction. The distillation involves both 3D volumetric supervision and 2D rendering supervision from virtual novel views. To deal with inherent ambiguities in occluded regions, our model also predicts 3D uncertainty. During both scene generation and distillation, we exclusively rely on single image and do not require multi-view data or 3D supervision.

Experiments on the challenging KITTI-360 [31] and Waymo [54] datasets show that our distilled model is competitive with state-of-the-art methods for monocular 3D reconstruction using multi-view supervision. Furthermore, we show that our method has unique advantages when it comes to dynamic scenes. Through extensive ablation stud-

ies, we validate the effectiveness of our design choices both for scene generation and distillation. Our contributions are:

- A specialized *view completion model* that inpaints and refines synthetic novel views and which can be trained using only a single image per scene.
- A *synthetic occupancy field* formulation to construct dense scene geometry from multiple synthetic views.
- A single-view *scene reconstruction model*, which is trained from the synthesized data and is competitive with reconstruction methods trained on multi-view data.

## 2. Related Work

### 2.1. Monocular depth prediction

The task of inferring depth information from a single image is a fundamental challenge in computer vision. Early works trained neural networks in a supervised way to directly regress relative depth for specific domains, *e.g.* autonomous driving [8, 9, 11, 15, 26, 33, 57]. Some works avoided the need for explicit supervision and relied on self-supervised loss formulations based on multi-view consistency [13, 14]. As one of the first, Midas [44] proposed a training formulation that allows effective training on many diverse datasets at the same time, shifting the focus to build more general-purpose monocular relative depth prediction networks. A number of follow-up approaches have since improved different parts of the pipeline [1, 45, 62–64]. Most recently, several works [2, 20, 38, 65], notably Metric3D [20] and UniDepth [38], proposed methods for general-purpose *metric* depth prediction. As monocular depth prediction methods have matured over the years, many applications now use such models in an off-the-shelf fashion.

### 2.2. Scene as occupancy

While depth predictions are useful, they only capture 2.5D information about the scene and do not provide details in *e.g.* occluded regions. Recently, a new line of work started training neural networks to directly infer a volumetric reconstruction from a single image [4, 5, 60]. Volumetric reconstructions allow to determine binary occupancy values for any point in the observed camera frustum. In general, the scene is either represented as a dense voxel grid [4, 28, 30, 35, 53], a continuous density field [5, 16, 27, 37, 60], or hybrid approaches like tri-planes [21, 22]. To obtain ground truth data for supervision, many works accumulate Lidar scans from a moving sensor over time [21, 28, 30, 35, 53]. Other approaches use losses on multi-view supervision and photometric consistency and can thus avoid the need for explicit 3D data [5, 16, 22, 27, 37, 60].

In general, methods for volumetric reconstruction from a single image require complex sensor setups to generate training data. This limits the scale of these datasets and

makes generalization challenging. Furthermore, they struggle with dynamic objects which violate the static scene assumption. Many approaches either ignore [60] or filter out [37] dynamic objects at training time. In contrast, our approach can be trained using single images and can deal with dynamic objects by design. It only requires an off-the-shelf diffusion model and depth prediction model.

### 2.3. 3D scene generation

Following the recent success of diffusion models for image generation [6, 39, 43, 47, 48], researchers also aimed to create powerful 3D generative models. However, similar to 3D reconstruction, the amount of training data available for 3D generation is limited. Consequently, models that directly generate 3D are restricted to object-centric content [19, 59].

Several lines of work propose to leverage 2D image generation models to improve 3D generation. Inspired by DreamBooth [40], some works [41, 50, 58] apply score distillation sampling (SDS) to generate 3D objects. However, such models are not stable and are thus still limited to object-centric 3D generation. Another promising direction [12, 18, 24, 34, 52, 55, 56, 59, 61] finetunes or retrains 2D diffusion models to generate multiple, 3D consistent views of a scene from different viewing directions. The generated views then enable 3D reconstruction in a second step. While these approaches often benefit from the generalization capabilities of pretrained 2D diffusion models, they are inherently limited. Besides requiring multi-view training data, the views that the models can generate are predefined and usually arranged in a circular pattern around an object in the center. Therefore, this line of work also struggles with unbounded in-the-wild scenes. Finally, a number of methods [7, 10, 17, 29, 32, 49, 51, 68] follow an iterative paradigm called *render-refine-repeat*. Every iteration is made up of two steps: 1) The current scene is *rendered* into an unobserved, virtual view, 2) the virtual view is *refined* (inpainted) using a 2D generative model and then lifted back into the scene using a pretrained depth prediction model. Earlier works like Infinite Nature [32] and Text2Room [17] represent the scene as 3D meshes, while more recent approaches use NeRFs [66] or Gaussian Splatting [7, 51]. Unlike this work, most approaches in that domain focus on novel-view-synthesis, which does not require perfect geometry.

## 3. Method

In the following, we first introduce our *view completion model* (VCM), which completes occlusions and removes artifacts in warped images. We then present how we apply the VCM in combination with a depth prediction network to iteratively synthesize 3D scene geometry in the form of a *synthetic occupancy field* (SOF) from just a single image. Finally, we describe how we distill these synthesized scenes into a lightweight feed-forward *scene reconstruction model*.

Fig. 2 provides a comprehensive overview.

### 3.1. Preliminaries

For a given scene, our method receives as input a single image  $\mathbf{I}_{\text{in}} \in ([0, 1]^3)^\Omega$ , where  $\Omega = \{1, \dots, H\} \times \{1, \dots, W\}$  denotes the grid of pixels. Through an off-the-shelf monocular depth prediction network, we can additionally obtain per-pixel depths  $\mathbf{D}_{\mathbf{I}} \in \mathbb{R}_+^\Omega$ . For a synthetic novel view  $\hat{\mathbf{I}}_i$ , let  $\mathbf{P}_i \in \text{SE3}$  be the camera pose and let  $\mathbf{P}_{i \rightarrow j}$  denote a relative camera pose between views  $i$  and  $j$ . For all views, we assume the same projection  $\pi(\mathbf{x}) : \mathbb{R}^3 \rightarrow \mathbb{R}^2$  and unprojection  $\pi^{-1}(\mathbf{p}, d) : (\mathbb{R}^2, \mathbb{R}_+) \rightarrow \mathbb{R}^3$  function, which map from 3D points  $\mathbf{x} \in \mathbb{R}^3$  to pixels  $\mathbf{p} \in \mathbb{R}^2$  with depth  $d_{\mathbf{p}} \in \mathbb{R}_+$ , and vice-versa. By combining  $\pi$  and  $\mathbf{P}$ , we can map a pixel from the input view into another view:

$$\mathbf{p}_i = \pi(\mathbf{P}_{\text{in} \rightarrow i} \pi^{-1}(\mathbf{p}_{\text{in}}, d_{\mathbf{p}_{\text{in}}})) \quad (1)$$

### 3.2. Training the View Completion Model

A single image only provides a partial observation of the 3D scene. We aim to use the ability of 2D generative models to inpaint realistic content given some context. Concretely, we follow the *render-refine-repeat* framework. First, the known scene content (*e.g.* the input image) is warped into a virtual novel view, where unknown regions remain empty. Then, a generative model fills in the empty or occluded regions conditioned on the known context and ideally removes artifacts. The now completed and refined view can be lifted into 3D again to refine the scene. However, naively applying an inpainting diffusion model like StableDiffusion-2.1 yields insufficient inpainting quality. This is because the views found in *e.g.* autonomous driving differ significantly from the ones the model was originally trained on, which tend to be casual photos. Therefore, we rely on a specialized *view completion model* (VCM).

The VCM is implemented as a ControlNet [67] for a pretrained StableDiffusion-2.1-unCLIP diffusion model. Rich conditioning and the correct parameterization are very important for effective view completion. Thus, the VCM receives as input the warped RGB, the (incomplete) depth representing the current scene geometry, and an inpainting mask. We mask out areas for inpainting with random noise in all inputs and apply morphological closing to the mask. Additionally, we provide the model with the CLIP [42] embedding of the input image. From this input, the VCM produces an inpainted and refined image.

The VCM needs to be trained using ground-truth pairs of conditioning and target image. Since we have only a single image per scene available, we take inspiration from [3] and design a training scheme based on forward-backward warping. Given an input image  $\mathbf{I}_{\text{in}}$  and predicted depth  $\mathbf{D}_{\mathbf{I}_{\text{in}}}$ , we first warp the pixels into a virtual novel view with a random camera pose. Then, the virtual view is warped back into

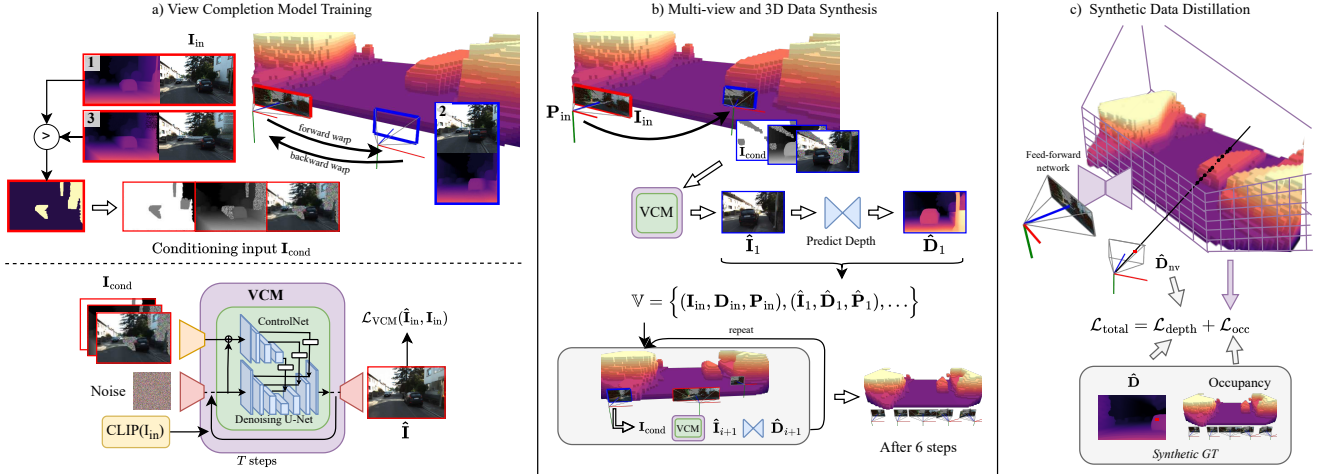


Figure 2. **Method overview.** **a)** We train a view completion model (VCM) that inpaints occluded areas and refines warped views. Training uses only a single view per scene and leverages forward-backward warping for data generation. **b)** The VCM is applied iteratively alongside a depth prediction network to synthesize virtual novel views, enabling progressive refinement of the 3D geometry. **c)** The synthesized scene geometries are then used to distill a feed-forward scene reconstruction model, by supervising occupancy and virtual depth.

the input camera pose. For areas of the input image, which would be occluded in the novel view, the backward warped image will be corrupted. We can find these occluded regions by doing a per-pixel comparison of the back-projected depth with the original depth. If the reprojected depth is lower for a pixel, then that pixel is occluded. Through this process, we create realistic occlusions and rendering artifacts to train the VCM. The warping uses the same rendering formulation as for synthesizing a new scene which is described in the following.

### 3.3. Synthesizing Scene Geometry

Within the *render-refine-repeat* framework, we generate several synthetic novel views, complete them using the VCM, predict corresponding depth maps, and update the scene geometry. To this end, we require a way to model scene geometry from the predicted depth maps, render novel views, and determine occlusions. Let  $\mathbb{V} = \{(\mathbf{I}_{in}, \mathbf{D}_{in}, \mathbf{P}_{in}), (\hat{\mathbf{I}}_1, \hat{\mathbf{D}}_1, \hat{\mathbf{P}}_1), \dots\}$  be the set of currently active view-depth-pose triplets. Initially,  $\mathbb{V}$  contains only the input view and is then extended via *render-refine-repeat*.

**Modeling scene geometry.** Throughout our approach, we consider a continuous *synthetic occupancy field*  $\Theta_{\mathbb{V}}(\mathbf{x}) : \mathbb{R}^3 \rightarrow \{0, 1\}$ , which maps every point  $\mathbf{x} \in \mathbb{R}^3$  in the scene to a binary occupancy value and which depends on  $\mathbb{V}$ . Intuitively, a point  $\mathbf{x}$  is regarded as not occupied if it lies *in front* of the predicted depth of *any* active view, for which it is in the camera frustum. Conversely, if it lies behind the predicted depth for *all* views, it is considered occupied. Let  $\mathbf{x}_i = \mathbf{P}_i \mathbf{x}$  be the point transformed into the coordinate system of view  $i$ ,  $\mathbf{p}_i = \pi(\mathbf{x}_i)$  the corresponding pixel after

projection to the image plane, and  $d_{\mathbf{p}_i}$  the predicted depth at that pixel. We determine the occupancy of  $\mathbf{x}$  through the following logical formula:

$$\theta_i^{\text{inside-frustum}}(\mathbf{x}) = [\mathbf{p}_i \in \Omega] \quad (2)$$

$$\theta_i^{\text{behind-depth}}(\mathbf{x}) = [\mathbf{x}_i^z > d_{\mathbf{p}_i}] \quad (3)$$

$$\theta_i^{\text{occ}}(\mathbf{x}) = \theta_i^{\text{inside-frustum}}(\mathbf{x}) \wedge \theta_i^{\text{behind-depth}}(\mathbf{x}) \quad (4)$$

$$\Theta_{\mathbb{V}}(\mathbf{x}) = \bigwedge_{i \in \mathbb{V}} \theta_i^{\text{occ}}(\mathbf{x}) \quad (5)$$

**Rendering novel views.** We rely on the established volume rendering formulation [23], popularized in recent years by NeRF [36]. Here, an image is rendered by casting a ray for every pixel from the camera into 3D space. The ray is evaluated at discrete steps  $\mathbf{x}$  for density  $\sigma(\mathbf{x})$  and color  $c(\mathbf{x})$ . The final pixel color is determined by integrating over the density along the ray.

In our case, we can directly use our binary occupancy as density:  $\sigma(\mathbf{x}) = \Theta_{\mathbb{V}}(\mathbf{x})$ . Because color information is not defined in 3D space, we sample it from the 2D views. When projecting  $\mathbf{x}$  into view  $i$  and obtaining pixel location  $\mathbf{p}_i$ , let  $c_i$  be the corresponding pixel color. However, not all  $c_i$  are valid, as the 3D point could be occluded or in empty space in the image. To aggregate the sampled color values, we use a heuristic: If  $\mathbf{x}$  is closer than a threshold  $\tau_s$  to a surface in view  $i$ , then it is likely valid. The final color is obtained by averaging all valid color values:

$$\theta_i^{\text{surface}}(\mathbf{x}) = [|\mathbf{x}_i^z - d_{\mathbf{p}_i}| < \tau_s] \wedge \theta_i^{\text{inside-frustum}}(\mathbf{x}) \quad (6)$$

$$c(\mathbf{x}) = \frac{\sum_{i \in \mathbb{V}} c_i \cdot \theta_i^{\text{surface}}(\mathbf{x})}{\sum_{i \in \mathbb{V}} \theta_i^{\text{surface}}(\mathbf{x})} \quad (7)$$

Let  $\tilde{\mathbf{I}}_{\text{nv}}$  denote the rendered view, which can contain invalid regions (due to occlusions) and sampling artifacts. By computing the expected ray termination depth (which in our case corresponds to where a ray hits occupancy for the first time), we can also render a depth map  $\tilde{\mathbf{D}}_{\text{nv}}$ .

**Detecting occlusions in novel views.** When warping one view into another and the viewpoint change is limited, then sharp changes in the reference depth map serve as a good proxy for which regions will introduce occlusions. We leverage this aspect and compute a depth gradient map using Sobel filters on the inverse depth map, which highlights regions with significant depth changes. Subsequently, a threshold  $\tau_d$  is applied to binarize the map.

$$\mathbf{O}_i = \sqrt{\left(\frac{\partial}{\partial x} \mathbf{D}_i\right)^2 + \left(\frac{\partial}{\partial y} \mathbf{D}_i\right)^2} > \tau_d \quad (8)$$

We finally render it alongside the RGB color channels into the novel view to obtain  $\mathbf{O}_{\text{nv}}$ . In a post-processing step, we apply morphological opening to remove isolated noise followed by morphological closing join neighboring patches.

**Sampling and completing novel views.** By adding more views to the set of active views  $\mathbb{V}$ , we refine the scene geometry represented by the synthetic occupancy field. The better the views cover different areas of the scene, the better the resulting geometry will be. Therefore, we predefine a set  $\mathbb{P} = \{\mathbf{P}_1, \dots, \mathbf{P}_{n_{\text{synth}}}\}$  of camera poses for synthetic novel views. For every view  $j \in \mathbb{P}$ , we render the RGB  $\tilde{\mathbf{I}}_j$ , depth  $\tilde{\mathbf{D}}_j$ , and occlusions  $\mathbf{O}_j$ . From this conditioning, the VCM then inpaints and refines the incomplete view, resulting in the synthetic novel view  $\hat{\mathbf{I}}_j$ . Finally, we apply the depth predictor to obtain the completed depth map  $\hat{\mathbf{D}}_j$  and we can update  $\mathbb{V}$  with the triplet  $(\hat{\mathbf{I}}_j, \hat{\mathbf{D}}_j, \hat{\mathbf{P}}_j)$ .

### 3.4. Distilling into a Scene Reconstruction Model

While we can synthesize high-quality scene geometry using the view completion model, the process is expensive and not suitable for real-time applications. Furthermore, the pipeline involves several independent components, which makes it prone to artifacts. To address these limitations, we generate scene geometry for all images of a dataset and distill a feed-forward *scene reconstruction model*. Given a single image as input, it predicts a discretized occupancy field  $\Theta_{\text{SRM}} \in [0, 1]^{Z \times H \times W}$ . However, there is an inherent ambiguity when generating or reconstructing scenes from a single image. Therefore, we also predict an uncertainty field  $\omega \in \mathbb{R}_+^{Z \times H \times W}$ .

The training involves two loss terms. First, we directly supervise the predicted occupancy. Concretely, we rely on an uncertainty-based loss formulation inspired by [25],

which is self-calibrating.

$$\mathcal{L}_{\text{occ}}(\Theta_{\text{SRM}}, \Theta) = \sum_{\mathbf{x}} \frac{(\Theta(\mathbf{x}) - \Theta_{\text{SRM}}(\mathbf{x}))^2}{\omega(\mathbf{x})} + \log \omega(\mathbf{x}) \quad (9)$$

Additionally, we render depth maps  $\tilde{\mathbf{D}}_i$  using our  $\Theta_{\text{SRM}}$  from the same camera poses as the synthetic views in  $\mathbb{V}$ . We then directly supervise them via the depth predictions  $\mathbf{D}_i$  from  $\mathbb{V}$  using a Gaussian Negative Log-Likelihood (GNLL) loss, as proposed in [46]. The loss term provides training signals to the surface areas of the predicted density field, which are particularly hard to learn.

$$\mathcal{L}_{\text{depth}} = \sum_{i \in \mathbb{V}} \text{GNLL}(\tilde{\mathbf{D}}_i, \mathbf{D}_i) \quad (10)$$

The final loss is then a weighted sum:

$$\mathcal{L} = \lambda_{\text{occ}} \mathcal{L}_{\text{occ}} + \lambda_{\text{depth}} \mathcal{L}_{\text{depth}}. \quad (11)$$

## 4. Experiments

To demonstrate the capabilities of our approach, we conduct extensive experiments regarding volumetric scene reconstruction both for the synthesized scenes and the distilled reconstruction model. Furthermore, we carefully validate our design choices for the view completion model, scene synthesis, and distillation procedure.

### 4.1. Setup

**Data.** We test our method on the challenging KITTI-360 [31] and Waymo [54] self-driving datasets. Both datasets contain scenes with complex layouts and possibly dynamic objects. While they provide multi-view data, we use only a single view per scene both for training and testing. For KITTI-360, we load images at  $384 \times 1280$  resolution during View Completion Model training and at  $192 \times 640$  resolution otherwise. On Waymo, we use images at a resolution of  $320 \times 480$ .

**Implementation details.** For the depth predictor, we rely on Metric3D [65]. The scene reconstruction model adopts the ResNet50-based U-Net backbone from [60]. We add batch-normalization layers to the backbone’s decoder to stabilize mixed-precision training. The predicted occupancy field has a resolution  $Z = 64$ , inversely spaced between  $3m$  and  $50m$ . The training takes approximately 2 days for the View Completion Model and 3 days for the reconstruction model on 4 Nvidia A100 GPUs. For more details regarding data setup and training, please refer to the supplementary material.

Method	Learns occlusions	No multi-view data	KITTI-360 [31]			Waymo [54]		
			O <sub>acc</sub> ↑	IE <sub>acc</sub> ↑	IE <sub>rec</sub> ↑	O <sub>acc</sub> ↑	IE <sub>acc</sub> ↑	IE <sub>rec</sub> ↑
UniDepth* [38]	✗	✓	0.89	–	–	0.96	–	–
Metric3D-ViT-Large* [65]	✗	✓	0.91	–	–	<b>0.97</b>	–	–
BTS* [60]	✓	✗	0.92	0.69	0.64	0.95	0.63	0.94
BTS + depth supervision	✓	✗	0.92	0.70	0.66	0.95	0.61	<b>0.96</b>
KYN† [27]	✓	✗	0.92	0.70	0.72	–	–	–
<b>Ours</b>	✓	✓	<b>0.93</b>	<b>0.72</b>	<b>0.75</b>	<b>0.97</b>	<b>0.73</b>	<b>0.96</b>
<b>Ours (Distilled)</b>	✓	✓	0.90	0.71	0.71	0.96	0.72	0.93

Table 1. **Quantitative scene reconstruction.** We report scene geometry estimation results using ground-truth derived from accumulated LiDAR scans and semantic annotations on KITTI-360 and Waymo. Both the synthesized scenes and the distilled model match or surpass baselines, despite not requiring multi-view training data. **Legend:** ✗: official checkpoint, †: results as reported in the reference.

**Evaluation procedure.** We use 2D reconstruction metrics to evaluate image synthesis results in the input camera’s viewpoint, where ground truth is available. Here, PSNR measures reconstruction quality of RGB images, and absolute relative error (Abs Rel) is used for depth. When evaluating novel view quality, we apply refinement in the novel view and then re-project the refined views into the input view to compute the metrics w.r.t. the input image (masking out invalid pixels).

Furthermore, we rely on the established occupancy evaluation strategy using LiDAR GT from [27, 60] to evaluate 3D consistency of novel views and the quality of the 3D reconstruction in an area of dimension  $x = [-4m, 4m]$ ,  $y = [-1m, 0m]$ ,  $z = [4m, 20m]$ . On Waymo, we augment the LiDAR GT with occupancy from object bounding boxes to keep dynamic objects. We evaluate the overall accuracy of the reconstruction  $O_{acc}$ , as well as the accuracy and recall of the reconstruction in invisible and empty regions (*i.e.* behind the visible surface in the input image).

## 4.2. Scene Reconstruction

We first test our method’s ability to generate accurate volumetric geometry from a single image in complex scenes. Here, the state-of-the-art volumetric reconstruction methods Behind the Scenes (BTS) [60] and Know Your Neighbor (KYN) [27] serve as baselines. Both use multi-view supervision from all cameras and multiple time steps. Because our approach uses an off-the-shelf depth predictor to synthesize geometry, we also train a second BTS baseline that uses depth prediction in addition to multi-view supervision. This ensures similar priors and a fair comparison. Furthermore, we test the recent MDE models UniDepth [38] and Metric3D [20]. Since depth prediction cannot reason about occluded areas, we do not report the  $IE_{acc}$  and  $IE_{rec}$  metrics.

As shown in Tab. 1, compared to previous methods, our reconstructed synthetic occupancy field achieve the best overall reconstruction ( $O_{acc}$ ) and the best reconstruction of invisible and empty regions ( $IE_{acc}$  and  $IE_{rec}$ ). Our distilled scene reconstruction model matches the performance

of KYN and surpasses BTS [60], despite using only single images. Even with depth supervision, BTS performance still lags behind. We hypothesize that this lack of improvement stems from the strong depth cues already inherent in multi-view data. In fact, inconsistent depth predictions with slightly varying scales may even harm BTS training.

We visualize the scene geometry by discretizing the occupancy into a voxel grid. As illustrated in Fig. 3, both the synthesized scenes and the geometry predicted by the scene reconstruction model exhibit high overall quality. However, the synthesized scenes occasionally display artifacts caused by poor view completion or depth prediction. The distilled scene reconstruction model does not exhibit these issues, as it is trained on a diverse dataset. We contend that, despite being slightly outperformed in quantitative metrics by the directly synthesized geometry, the distilled model is more reliable and significantly faster. As shown in the 3rd and 4th columns, both BTS variants fail to reconstruct the dynamic object. This failure stems from their use of multi-view data across multiple timesteps, which introduces inconsistency when the object is in motion. In contrast, our synthesized scenes naturally handle such scenarios.

## 4.3. Scene Synthesis using the VCM

The process of synthesizing scene geometry – by generating novel views and fusing depth maps – relies on multiple components that significantly influence the final result’s quality. To this end, we rigorously validate our design choices through a series of ablation studies.

### 4.3.1. Conditioning of the VCM

Our VCM receives a range of conditioning inputs. To assess the impact of conditioning, we compare our full VCM model against a simplified variant, denoted as  $VCM^{simple}$ . This simplified configuration receives only the RGB input, where the region to be inpainted is masked with zeros instead of noise. We evaluate both configurations on the KITTI-360 dataset ( $VCM^K$ ), and further examine the effect of finetuning on Waymo ( $VCM^{K \rightarrow W}$ ).

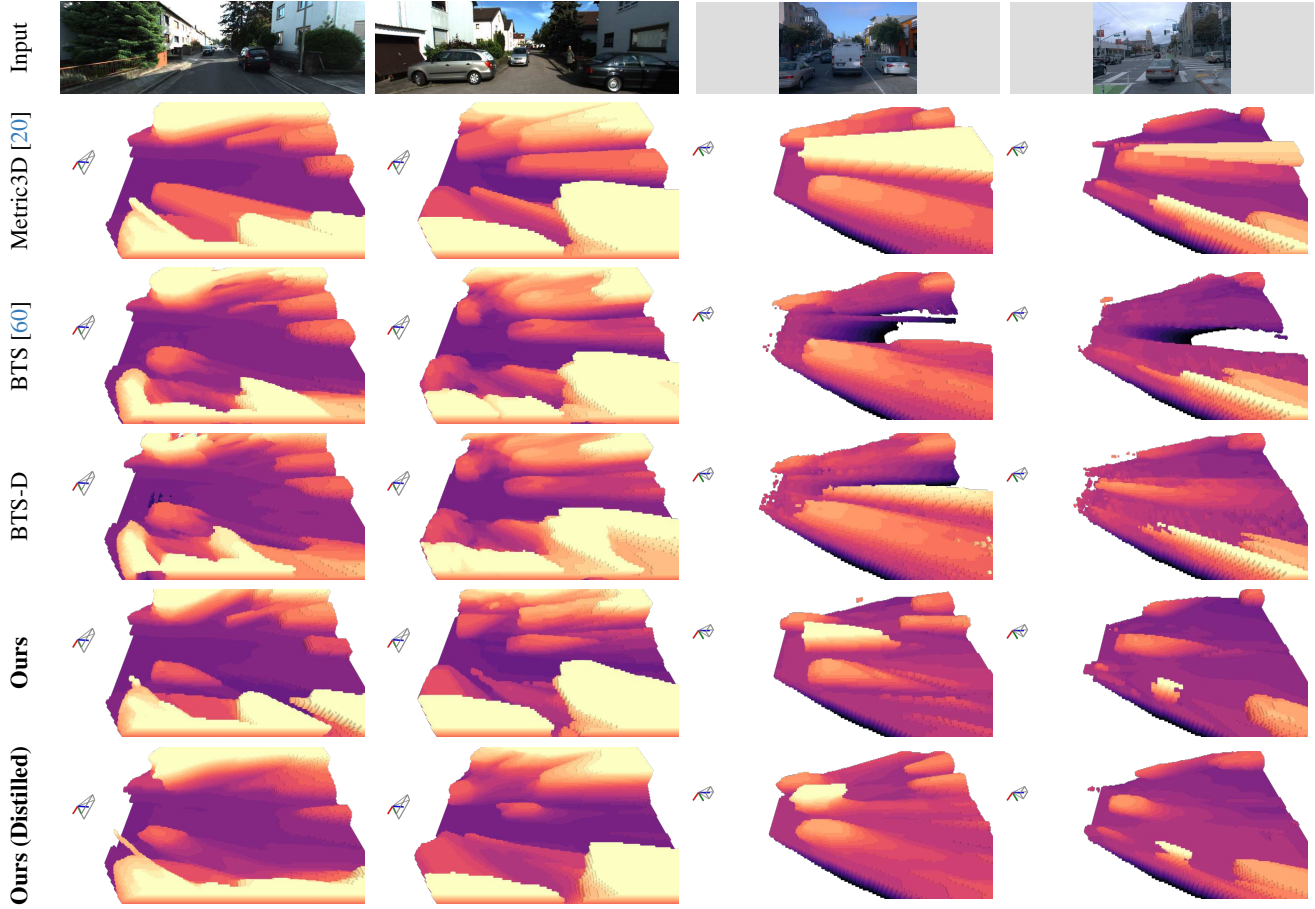


Figure 3. **Qualitative scene reconstruction.** We present scene reconstructions from several models on KITTI-360 [31] (left) and Waymo [54] (right). The geometry is discretized into a voxel grid with dimensions  $x = [-9m, 9m]$ ,  $y = [-0.25m, 4m]$ ,  $z = [4m, 25m]$ . The color in the plots indicates the y-coordinate (up-axis). Despite being trained on single images only, our method achieves accurate reconstructions overall. In addition, it reliably reconstructs dynamic objects, and the distilled model effectively avoids artifacts.

Method	Input View		Novel View	
	PSNR $\uparrow$	Abs Rel $\downarrow$	PSNR $\uparrow$	Abs Rel $\downarrow$
<i>KITTI-360</i>				
VCM <sup>simple</sup>	20.197	0.174	21.323	0.154
VCM <sup>K</sup>	<b>23.908</b>	<b>0.161</b>	<b>23.394</b>	<b>0.135</b>
<i>Waymo</i>				
VCM <sup>K</sup>	26.963	0.286	21.432	0.177
VCM <sup>K<math>\rightarrow</math>W</sup>	<b>28.781</b>	<b>0.260</b>	<b>22.603</b>	<b>0.135</b>

Table 2. **Effect of VCM conditioning.** We evaluate different model configurations and training setups. VCM<sup>simple</sup> receives only masked RGB input. VCM<sup>K</sup> and VCM<sup>K $\rightarrow$ W</sup> denote the full model trained on KITTI-360 and finetuned on Waymo, respectively.

As shown in Tab. 2, the full model consistently outperforms the baseline in both color and depth reconstruction metrics on KITTI-360. On Waymo, finetuning clearly enhances reconstruction quality even further.

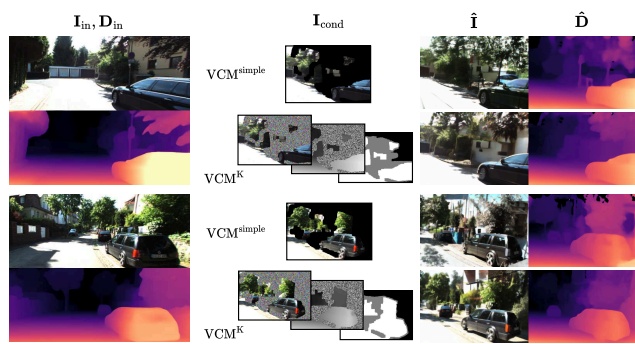


Figure 4. **Effect of VCM conditioning.** See Tab. 2.

### 4.3.2. Occlusion detection in novel views

The accuracy and robustness of our occlusion detection strategy directly influence the effectiveness of refining incomplete novel views using VCM. We compare our depth-gradient-based method against an alternative approach that

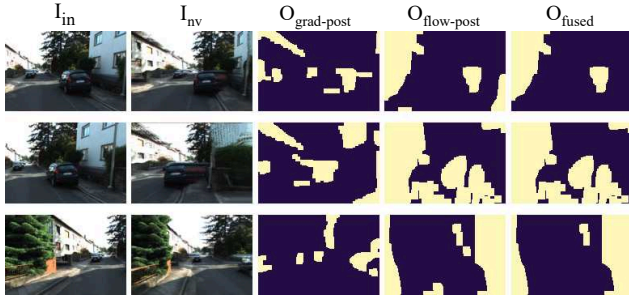


Figure 5. **Effect of occlusion detection strategies.** We compare gradient-based (ours) to optical-flow based occlusion detection, and a combination of both. Occlusions are shown in **yellow**.

Pose sampling	$ \mathbb{P} $	$O_{\text{acc}} \uparrow$	$IE_{\text{acc}} \uparrow$	$IE_{\text{rec}} \uparrow$
Random orbit	4	0.923	0.674	0.596
Random shift	4	0.927	0.692	0.636
Rig	4	0.930	0.708	0.687
<b>Rig</b>	<b>8</b>	<b>0.932</b>	<b>0.720</b>	<b>0.729</b>

Table 3. **Pose sampling strategies.** We evaluate the quality of generated geometry under various pose sampling strategies. A camera rig with eight predefined poses and random rotations achieves the best performance.

leverages two-way optical flow between the input and novel views to identify regions visible only in the latter, as well as a conservative fusion of both techniques. As shown in Fig. 5, the depth gradient method robustly captures occlusions without requiring extensive post-filtering. In contrast, the optical flow approach introduces numerous false positives in the presence of large warps, necessitating aggressive filtering that subsequently reduces true positive detections. Moreover, it incorrectly classifies all pixels outside the input view’s field of view as occluded. The fused strategy mitigates some of the false positives compared to optical flow alone but still inherits many of its limitations.

#### 4.3.3. Viewpoint sampling

The selection of poses for novel views has a substantial impact on 3D scene geometry reconstruction, especially in occluded regions. We evaluate several pose sampling strategies using our occupancy reconstruction benchmark. As shown in Tab. 3, translating the camera along the input baseline by  $[-3m, 3m]$  yields better results than orbiting it by  $[-10^\circ, 10^\circ]$  around a vertical axis at a depth of  $5m$ . Camera rigs outperform random warp sampling strategies, as their cameras are already defined in sensible poses.

#### 4.4. Distillation into a Feed-Forward Model

The loss configuration used to distill synthetic data into the scene reconstruction model is critical to its performance. We assess the contribution of individual loss terms by evaluating occupancy reconstruction metrics in Tab. 4 and providing qualitative comparisons in Fig. 6. Compared to ab-

Method	$O_{\text{acc}} \uparrow$	$IE_{\text{acc}} \uparrow$	$IE_{\text{rec}} \uparrow$
<b>Full</b>	<b>0.902</b>	<b>0.705</b>	<b>0.706</b>
w/o $\mathcal{L}_{\text{depth}}$	0.857	0.656	0.443
w/o $\mathcal{L}_{\text{occ}}$	<b>0.907</b>	<b>0.699</b>	<b>0.757</b>
w/o uncertainty	<b>0.907</b>	0.697	0.701

Table 4. **Quantitative effect of different loss terms.** We show reconstructions produced by models with different loss terms turned off. Overall, the full model produces the most convincing results.

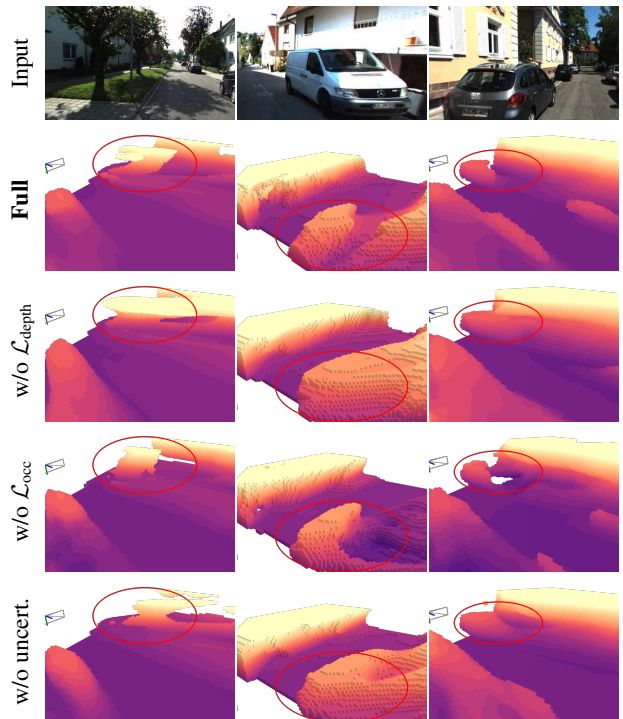


Figure 6. **Qualitative effect of different loss terms.** See Tab. 4.

lated variants, our *full* loss setup achieves competitive  $O_{\text{acc}}$  and the highest  $IE_{\text{acc}}$ . While removing  $\mathcal{L}_{\text{occ}}$  increases the invisible and empty region recall ( $IE_{\text{rec}}$ ), it lowers  $IE_{\text{acc}}$  – indicating that the model over-predicts free space, which may not be correct. Moreover, the predicted uncertainty is needed to balance the depth and volumetric loss w.r.t. each other. As illustrated in Fig. 6, omitting  $\mathcal{L}_{\text{depth}}$  leads to less accurate reconstruction of invisible and empty regions. Eliminating  $\mathcal{L}_{\text{occ}}$  worsens the reconstruction of invisible but non-empty space, an effect not reflected in  $IE_{\text{rec}}$ . Finally, the predicted uncertainty is essential for balancing the depth and volumetric losses relative to one another.

## 5. Conclusion

In this work, we proposed a novel approach to monocular 3D reconstruction that can be trained using only single images. The resulting geometry matches or exceeds the performance of models trained with multi-view supervision.

**Acknowledgements:** This work was funded by the ERC Advanced Grant "SIMULACRON" (agreement #884679), the GNI Project "AI4Twinning", and the DFG project CR 250/26-1 "4D YouTube".

## References

- [1] Shariq Farooq Bhat, Reiner Birkel, Diana Wofk, Peter Wonka, and Matthias Müller. Zoedepth: Zero-shot transfer by combining relative and metric depth. *arXiv preprint arXiv:2302.12288*, 2023. 1, 2
- [2] Aleksei Bochkovskii, Amaël Delaunoy, Hugo Germain, Marcel Santos, Yichao Zhou, Stephan R Richter, and Vladlen Koltun. Depth pro: Sharp monocular metric depth in less than a second. *arXiv preprint arXiv:2410.02073*, 2024. 2
- [3] Shengqu Cai, Eric Ryan Chan, Songyou Peng, Mohamad Shahbazi, Anton Obukhov, Luc Van Gool, and Gordon Wetzstein. Diffdreamer: Towards consistent unsupervised single-view scene extrapolation with conditional diffusion models. In *ICCV*, 2023. 3
- [4] Anh-Quan Cao and Raoul De Charette. Monoscene: Monocular 3d semantic scene completion. In *Proceedings of the IEEE/CVF Conference on Computer Vision and Pattern Recognition*, pages 3991–4001, 2022. 1, 2
- [5] Anh-Quan Cao and Raoul De Charette. Scenerf: Self-supervised monocular 3d scene reconstruction with radiance fields. In *Proceedings of the IEEE/CVF International Conference on Computer Vision*, pages 9387–9398, 2023. 2
- [6] Junsong Chen, Jincheng Yu, Chongjian Ge, Lewei Yao, Enze Xie, Yue Wu, Zhongdao Wang, James Kwok, Ping Luo, Huchuan Lu, et al. Pixart- $\alpha$ : Fast training of diffusion transformer for photorealistic text-to-image synthesis. *arXiv preprint arXiv:2310.00426*, 2023. 3
- [7] Jaeyoung Chung, Suyoung Lee, Hyeongjin Nam, Jaerin Lee, and Kyoung Mu Lee. Luciddreamer: Domain-free generation of 3d gaussian splatting scenes. *arXiv preprint arXiv:2311.13384*, 2023. 2, 3
- [8] David Eigen and Rob Fergus. Predicting depth, surface normals and semantic labels with a common multi-scale convolutional architecture. In *Proceedings of the IEEE international conference on computer vision*, pages 2650–2658, 2015. 2
- [9] David Eigen, Christian Puhrsch, and Rob Fergus. Depth map prediction from a single image using a multi-scale deep network. *Advances in neural information processing systems*, 27, 2014. 2
- [10] Paul Engstler, Andrea Vedaldi, Iro Laina, and Christian Rupprecht. Invisible stitch: Generating smooth 3d scenes with depth inpainting. *arXiv preprint arXiv:2404.19758*, 2024. 3
- [11] Huan Fu, Mingming Gong, Chaohui Wang, Kayhan Batmanghelich, and Dacheng Tao. Deep ordinal regression network for monocular depth estimation. In *Proceedings of the IEEE conference on computer vision and pattern recognition*, pages 2002–2011, 2018. 2
- [12] Ruiqi Gao, Aleksander Holynski, Philipp Henzler, Arthur Brussee, Ricardo Martin-Brualla, Pratul Srinivasan, Jonathan T Barron, and Ben Poole. Cat3d: Create anything in 3d with multi-view diffusion models. *arXiv preprint arXiv:2405.10314*, 2024. 3
- [13] Clément Godard, Oisín Mac Aodha, and Gabriel J Brostow. Unsupervised monocular depth estimation with left-right consistency. In *Proceedings of the IEEE conference on computer vision and pattern recognition*, pages 270–279, 2017. 2
- [14] Clément Godard, Oisín Mac Aodha, Michael Firman, and Gabriel J Brostow. Digging into self-supervised monocular depth estimation. In *Proceedings of the IEEE/CVF international conference on computer vision*, pages 3828–3838, 2019. 2
- [15] Vitor Guizilini, Rares Ambrus, Wolfram Burgard, and Adrien Gaidon. Sparse auxiliary networks for unified monocular depth prediction and completion. In *Proceedings of the IEEE/CVF conference on computer vision and pattern recognition*, pages 11078–11088, 2021. 2
- [16] Adrian Hayler, Felix Wimbauer, Dominik Muhle, Christian Rupprecht, and Daniel Cremers. S4c: Self-supervised semantic scene completion with neural fields. In *2024 International Conference on 3D Vision (3DV)*, pages 409–420. IEEE, 2024. 2
- [17] Lukas Höllein, Ang Cao, Andrew Owens, Justin Johnson, and Matthias Nießner. Text2room: Extracting textured 3d meshes from 2d text-to-image models. In *Proceedings of the IEEE/CVF International Conference on Computer Vision*, pages 7909–7920, 2023. 2, 3
- [18] Lukas Höllein, Aljaž Božič, Norman Müller, David Novotny, Hung-Yu Tseng, Christian Richardt, Michael Zollhöfer, and Matthias Nießner. Viewdiff: 3d-consistent image generation with text-to-image models. In *Proceedings of the IEEE/CVF conference on computer vision and pattern recognition*, pages 5043–5052, 2024. 3
- [19] Yicong Hong, Kai Zhang, Jiuxiang Gu, Sai Bi, Yang Zhou, Difan Liu, Feng Liu, Kalyan Sunkavalli, Trung Bui, and Hao Tan. Lrm: Large reconstruction model for single image to 3d. *arXiv preprint arXiv:2311.04400*, 2023. 3
- [20] Mu Hu, Wei Yin, Chi Zhang, Zhipeng Cai, Xiaoxiao Long, Hao Chen, Kaixuan Wang, Gang Yu, Chunhua Shen, and Shaojie Shen. Metric3d v2: A versatile monocular geometric foundation model for zero-shot metric depth and surface normal estimation. *IEEE Transactions on Pattern Analysis and Machine Intelligence*, 2024. 2, 6, 7
- [21] Yuanhui Huang, Wenzhao Zheng, Yunpeng Zhang, Jie Zhou, and Jiwen Lu. Tri-perspective view for vision-based 3d semantic occupancy prediction. In *Proceedings of the IEEE/CVF conference on computer vision and pattern recognition*, pages 9223–9232, 2023. 2
- [22] Yuanhui Huang, Wenzhao Zheng, Borui Zhang, Jie Zhou, and Jiwen Lu. Selfocc: Self-supervised vision-based 3d occupancy prediction. In *Proceedings of the IEEE/CVF Conference on Computer Vision and Pattern Recognition*, pages 19946–19956, 2024. 2
- [23] James T Kajiya and Brian P Von Herzen. Ray tracing volume densities. *ACM SIGGRAPH computer graphics*, 18(3):165–174, 1984. 4

- [24] Animesh Karnewar, Andrea Vedaldi, David Novotny, and Niloy J Mitra. Holodiffusion: Training a 3d diffusion model using 2d images. In *Proceedings of the IEEE/CVF conference on computer vision and pattern recognition*, pages 18423–18433, 2023. 3
- [25] Alex Kendall and Yarin Gal. What uncertainties do we need in bayesian deep learning for computer vision? *Advances in neural information processing systems*, 30, 2017. 5
- [26] Iro Laina, Christian Rupprecht, Vasileios Belagiannis, Federico Tombari, and Nassir Navab. Deeper depth prediction with fully convolutional residual networks. In *2016 Fourth international conference on 3D vision (3DV)*, pages 239–248. IEEE, 2016. 2
- [27] Rui Li, Tobias Fischer, Mattia Segu, Marc Pollefeys, Luc Van Gool, and Federico Tombari. Know your neighbors: Improving single-view reconstruction via spatial vision-language reasoning. In *Proceedings of the IEEE/CVF Conference on Computer Vision and Pattern Recognition*, pages 9848–9858, 2024. 1, 2, 6
- [28] Yiming Li, Zhiding Yu, Christopher Choy, Chaowei Xiao, Jose M Alvarez, Sanja Fidler, Chen Feng, and Anima Anandkumar. Voxformer: Sparse voxel transformer for camera-based 3d semantic scene completion. In *Proceedings of the IEEE/CVF conference on computer vision and pattern recognition*, pages 9087–9098, 2023. 1, 2
- [29] Zhengqi Li, Qianqian Wang, Noah Snavely, and Angjoo Kanazawa. Infinitenature-zero: Learning perpetual view generation of natural scenes from single images. In *European Conference on Computer Vision*, pages 515–534. Springer, 2022. 2, 3
- [30] Zhiqi Li, Zhiding Yu, David Austin, Mingsheng Fang, Shiyi Lan, Jan Kautz, and Jose M Alvarez. Fb-occ: 3d occupancy prediction based on forward-backward view transformation. *arXiv preprint arXiv:2307.01492*, 2023. 2
- [31] Yiyi Liao, Jun Xie, and Andreas Geiger. KITTI-360: A novel dataset and benchmarks for urban scene understanding in 2d and 3d. *Pattern Analysis and Machine Intelligence (PAMI)*, 2022. 2, 5, 7
- [32] Andrew Liu, Richard Tucker, Varun Jampani, Ameesh Makadia, Noah Snavely, and Angjoo Kanazawa. Infinite nature: Perpetual view generation of natural scenes from a single image. In *Proceedings of the IEEE/CVF International Conference on Computer Vision*, pages 14458–14467, 2021. 3
- [33] Fayao Liu, Chunhua Shen, Guosheng Lin, and Ian Reid. Learning depth from single monocular images using deep convolutional neural fields. *IEEE transactions on pattern analysis and machine intelligence*, 38(10):2024–2039, 2015. 2
- [34] Ruoshi Liu, Rundi Wu, Basile Van Hoorick, Pavel Tokmakov, Sergey Zakharov, and Carl Vondrick. Zero-1-to-3: Zero-shot one image to 3d object. In *Proceedings of the IEEE/CVF international conference on computer vision*, pages 9298–9309, 2023. 3
- [35] Ruihang Miao, Weizhou Liu, Mingrui Chen, Zheng Gong, Weixin Xu, Chen Hu, and Shuchang Zhou. Occdepth: A depth-aware method for 3d semantic scene completion. *arXiv preprint arXiv:2302.13540*, 2023. 2
- [36] Ben Mildenhall, Pratul P Srinivasan, Matthew Tancik, Jonathan T Barron, Ravi Ramamoorthi, and Ren Ng. Nerf: Representing scenes as neural radiance fields for view synthesis. *Communications of the ACM*, 65(1):99–106, 2021. 4
- [37] Mingjie Pan, Jiaming Liu, Renrui Zhang, Peixiang Huang, Xiaoqi Li, Hongwei Xie, Bing Wang, Li Liu, and Shanghang Zhang. Renderocc: Vision-centric 3d occupancy prediction with 2d rendering supervision. In *2024 IEEE International Conference on Robotics and Automation (ICRA)*, pages 12404–12411. IEEE, 2024. 1, 2, 3
- [38] Luigi Piccinelli, Yung-Hsu Yang, Christos Sakaridis, Mattia Segu, Siyuan Li, Luc Van Gool, and Fisher Yu. Unidepth: Universal monocular metric depth estimation. In *Proceedings of the IEEE/CVF Conference on Computer Vision and Pattern Recognition*, pages 10106–10116, 2024. 1, 2, 6
- [39] Dustin Podell, Zion English, Kyle Lacey, Andreas Blattmann, Tim Dockhorn, Jonas Müller, Joe Penna, and Robin Rombach. Sdxl: Improving latent diffusion models for high-resolution image synthesis. *arXiv preprint arXiv:2307.01952*, 2023. 3
- [40] Ben Poole, Ajay Jain, Jonathan T Barron, and Ben Mildenhall. Dreamfusion: Text-to-3d using 2d diffusion. *arXiv preprint arXiv:2209.14988*, 2022. 3
- [41] Guocheng Qian, Jinjie Mai, Abdullah Hamdi, Jian Ren, Aliaksandr Siarohin, Bing Li, Hsin-Ying Lee, Ivan Skokhodov, Peter Wonka, Sergey Tulyakov, et al. Magic123: One image to high-quality 3d object generation using both 2d and 3d diffusion priors. *arXiv preprint arXiv:2306.17843*, 2023. 3
- [42] Alec Radford, Jong Wook Kim, Chris Hallacy, Aditya Ramesh, Gabriel Goh, Sandhini Agarwal, Girish Sastry, Amanda Askell, Pamela Mishkin, Jack Clark, et al. Learning transferable visual models from natural language supervision. In *International conference on machine learning*, pages 8748–8763. PmlR, 2021. 3
- [43] Aditya Ramesh, Mikhail Pavlov, Gabriel Goh, Scott Gray, Chelsea Voss, Alec Radford, Mark Chen, and Ilya Sutskever. Zero-shot text-to-image generation. In *International conference on machine learning*, pages 8821–8831. Pmlr, 2021. 3
- [44] René Ranftl, Katrin Lasinger, David Hafner, Konrad Schindler, and Vladlen Koltun. Towards robust monocular depth estimation: Mixing datasets for zero-shot cross-dataset transfer. *IEEE transactions on pattern analysis and machine intelligence*, 44(3):1623–1637, 2020. 1, 2
- [45] René Ranftl, Alexey Bochkovskiy, and Vladlen Koltun. Vision transformers for dense prediction. In *Proceedings of the IEEE/CVF international conference on computer vision*, pages 12179–12188, 2021. 2
- [46] Barbara Roessle, Jonathan T Barron, Ben Mildenhall, Pratul P Srinivasan, and Matthias Nießner. Dense depth priors for neural radiance fields from sparse input views. In *Proceedings of the IEEE/CVF Conference on Computer Vision and Pattern Recognition*, pages 12892–12901, 2022. 5
- [47] Robin Rombach, Andreas Blattmann, Dominik Lorenz, Patrick Esser, and Björn Ommer. High-resolution image synthesis with latent diffusion models. In *Proceedings of*

- the *IEEE/CVF conference on computer vision and pattern recognition*, pages 10684–10695, 2022. 3
- [48] Chitwan Saharia, William Chan, Saurabh Saxena, Lala Li, Jay Whang, Emily L Denton, Kamyar Ghasemipour, Raphael Gontijo Lopes, Burcu Karagol Ayan, Tim Salimans, et al. Photorealistic text-to-image diffusion models with deep language understanding. *Advances in neural information processing systems*, 35:36479–36494, 2022. 3
- [49] Jonas Schult, Sam Tsai, Lukas Höllein, Bichen Wu, Jialiang Wang, Chih-Yao Ma, Kunpeng Li, Xiaofang Wang, Felix Wimbauer, Zijian He, et al. Controlroom3d: Room generation using semantic proxy rooms. In *Proceedings of the IEEE/CVF Conference on Computer Vision and Pattern Recognition*, pages 6201–6210, 2024. 3
- [50] Yichun Shi, Peng Wang, Jianglong Ye, Mai Long, Kejie Li, and Xiao Yang. Mvdream: Multi-view diffusion for 3d generation. *arXiv preprint arXiv:2308.16512*, 2023. 3
- [51] Jaidev Shriram, Alex Trevithick, Lingjie Liu, and Ravi Ramamoorthi. Realdreamer: Text-driven 3d scene generation with inpainting and depth diffusion. *arXiv preprint arXiv:2404.07199*, 2024. 3
- [52] Yawar Siddiqui, Tom Monnier, Filippos Kokkinos, Mahendra Kariya, Yanir Kleiman, Emilien Garreau, Oran Gafni, Natalia Neverova, Andrea Vedaldi, Roman Shapovalov, et al. Meta 3d assetgen: Text-to-mesh generation with high-quality geometry, texture, and pbr materials. *Advances in Neural Information Processing Systems*, 37:9532–9564, 2025. 3
- [53] Chonghao Sima, Wenwen Tong, Tai Wang, Li Chen, Silei Wu, Hanming Deng, Yi Gu, Lewei Lu, Ping Luo, Dahua Lin, et al. Scene as occupancy. *arXiv preprint arXiv:2306.02851*, 2023. 1, 2
- [54] Pei Sun, Henrik Kretzschmar, Xerxes Dotiwalla, Aurelien Chouard, Vijaysai Patnaik, Paul Tsui, James Guo, Yin Zhou, Yuning Chai, Benjamin Caine, Vijay Vasudevan, Wei Han, Jiquan Ngiam, Hang Zhao, Aleksei Timofeev, Scott Ettinger, Maxim Krivokon, Amy Gao, Aditya Joshi, Yu Zhang, Jonathon Shlens, Zhifeng Chen, and Dragomir Anguelov. Scalability in perception for autonomous driving: Waymo open dataset. In *Proceedings of the IEEE/CVF Conference on Computer Vision and Pattern Recognition (CVPR)*, 2020. 2, 5, 7
- [55] Stanislaw Szymanowicz, Christian Rupprecht, and Andrea Vedaldi. Viewset diffusion:(0-) image-conditioned 3d generative models from 2d data. In *Proceedings of the IEEE/CVF international conference on computer vision*, pages 8863–8873, 2023. 3
- [56] Jiayang Tang, Zhaoxi Chen, Xiaokang Chen, Tengfei Wang, Gang Zeng, and Ziwei Liu. Lgm: Large multi-view gaussian model for high-resolution 3d content creation. In *European Conference on Computer Vision*, pages 1–18. Springer, 2024. 3
- [57] Peng Wang, Xiaohui Shen, Zhe Lin, Scott Cohen, Brian Price, and Alan L Yuille. Towards unified depth and semantic prediction from a single image. In *Proceedings of the IEEE conference on computer vision and pattern recognition*, pages 2800–2809, 2015. 2
- [58] Zhengyi Wang, Cheng Lu, Yikai Wang, Fan Bao, Chongxuan Li, Hang Su, and Jun Zhu. Prolificdreamer: High-fidelity and diverse text-to-3d generation with variational score distillation. *Advances in Neural Information Processing Systems*, 36:8406–8441, 2023. 3
- [59] Xinyue Wei, Kai Zhang, Sai Bi, Hao Tan, Fujun Luan, Valentin Deschaintre, Kalyan Sunkavalli, Hao Su, and Zexiang Xu. Meshlrn: Large reconstruction model for high-quality meshes. *arXiv preprint arXiv:2404.12385*, 2024. 3
- [60] Felix Wimbauer, Nan Yang, Christian Rupprecht, and Daniel Cremers. Behind the scenes: Density fields for single view reconstruction. In *Proceedings of the IEEE/CVF Conference on Computer Vision and Pattern Recognition*, pages 9076–9086, 2023. 1, 2, 3, 5, 6, 7
- [61] Yinghao Xu, Zifan Shi, Wang Yifan, Hansheng Chen, Ceyuan Yang, Sida Peng, Yujun Shen, and Gordon Wetstein. Grm: Large gaussian reconstruction model for efficient 3d reconstruction and generation. In *European Conference on Computer Vision*, pages 1–20. Springer, 2024. 3
- [62] Lihe Yang, Bingyi Kang, Zilong Huang, Xiaogang Xu, Jiashi Feng, and Hengshuang Zhao. Depth anything: Unleashing the power of large-scale unlabeled data. In *Proceedings of the IEEE/CVF Conference on Computer Vision and Pattern Recognition*, pages 10371–10381, 2024. 2
- [63] Lihe Yang, Bingyi Kang, Zilong Huang, Zhen Zhao, Xiaogang Xu, Jiashi Feng, and Hengshuang Zhao. Depth anything v2. *Advances in Neural Information Processing Systems*, 37:21875–21911, 2025.
- [64] Wei Yin, Jianming Zhang, Oliver Wang, Simon Niklaus, Long Mai, Simon Chen, and Chunhua Shen. Learning to recover 3d scene shape from a single image. In *Proc. IEEE Conf. Comp. Vis. Patt. Recogn. (CVPR)*, 2021. 2
- [65] Wei Yin, Chi Zhang, Hao Chen, Zhipeng Cai, Gang Yu, Kaixuan Wang, Xiaozhi Chen, and Chunhua Shen. Metric3d: Towards zero-shot metric 3d prediction from a single image. In *Proceedings of the IEEE/CVF International Conference on Computer Vision*, pages 9043–9053, 2023. 1, 2, 5
- [66] Jingbo Zhang, Xiaoyu Li, Ziyu Wan, Can Wang, and Jing Liao. Text2nerf: Text-driven 3d scene generation with neural radiance fields. *IEEE Transactions on Visualization and Computer Graphics*, 30(12):7749–7762, 2024. 3
- [67] Lvmin Zhang, Anyi Rao, and Maneesh Agrawala. Adding conditional control to text-to-image diffusion models. In *IEEE International Conference on Computer Vision (ICCV)*, 2023. 3
- [68] Shijie Zhou, Zhiwen Fan, Dejie Xu, Haoran Chang, Pradyumna Chari, Tejas Bharadwaj, Suyu You, Zhangyang Wang, and Achuta Kadambi. Dreamscene360: Unconstrained text-to-3d scene generation with panoramic gaussian splatting. In *European Conference on Computer Vision*, pages 324–342. Springer, 2024. 3

# Supplementary Material

## Dream-to-Recon: Monocular 3D Reconstruction with Diffusion-Depth Distillation from Single Images

Philipp Wulff<sup>1</sup>

Felix Wimbauer<sup>1,2</sup>

Dominik Muhle<sup>1,2,3</sup>

Daniel Cremers<sup>1,2</sup>

<sup>1</sup>Technical University of Munich <sup>2</sup>MCML <sup>3</sup>SE3 Labs

[philippwulff.github.io/dream-to-recon](https://philippwulff.github.io/dream-to-recon)

In this supplementary material, we present additional implementation details, extended results, and ablation studies.

### A. Video Results

We include video results showcasing multiple sequences from both KITTI-360 and Waymo, available on our [project website](#). The videos illustrate per-frame volumetric reconstructions for our method alongside several baseline approaches.

### B. Implementation Details

**Model training.** Our view completion model is built upon Stable-Diffusion-2.1-unCLIP, employing the standard ControlNet architecture for conditioning. For training data synthesis, we render novel views at a resolution of  $192 \times 360$ , followed by re-rendering the input views at  $192 \times 288$ , which are then upsampled to  $512 \times 768$  to approximate the resolution used during the original training of Stable-Diffusion. The input image is derived from the re-rendered view. We use DDIM sampling during training and evaluate the model using UniPCMultiStep sampling with five steps. The training is initialized from the official Stable-Diffusion weights and runs for 20 epochs with a batch size of 20 and a constant learning rate of  $10^{-5}$ . During ControlNet training, UniDepth is used for depth prediction. However, subsequent experiments showed that Metric3D yields more accurate predictions than UniDepth; therefore, we adopt Metric3D for training the scene reconstruction model. To construct the pseudo-volume, we employ 48 coarse samples, 16 fine samples, and 16 ray samples placed within  $\sigma = 2$  of the estimated depth.

The scene reconstruction model architecture utilizes the ResNet50-based U-Net backbone from Behind the Scenes. To ensure stability in mixed-precision training, batch normalization layers are added to the decoder portion of the backbone. The backbone outputs a frustum-aligned density grid of dimensions  $192 \times 640 \times c$ , where  $c \in \{64, 128\}$ , with

an inverse growth pattern along the  $z$ -axis. The resulting occupancy field has a resolution of  $Z = 64$ , inversely spaced between depths of  $3m$  and  $50m$ .

Training is conducted using the UniPCMultiStepScheduler, with automatic mixed precision (AMP), caching, and batch size increases beginning from the second epoch.

**Ground truth for evaluation.** For each timestamp, a 3D occupancy grid is generated by removing all voxels that contain points from 300 consecutive LiDAR sweeps. The overall reconstruction accuracy ( $O_{acc}$ ) is computed within a cuboid defined by  $x = [-4m, 4m]$ ,  $y = [-0.75m, 0m]$ , and  $z = [4m, 20m]$  in the input camera’s coordinate frame. Given the higher frequency of dynamic objects in the Waymo dataset, we accumulate 300 LiDAR sweeps and retain occupancy only within the ground truth 3D bounding boxes. For Waymo, evaluation is performed on the validation set, as 3D bounding box annotations are not available in the test set.

Additionally, the metrics IEacc and IRec quantify the reconstruction’s accuracy and recall, respectively. These metrics are particularly important as they measure reconstruction quality *beyond* what a monocular depth estimation (MDE) model can typically achieve.

### C. Comparison With Render-Refine-Repeat Methods

Depth-based warping and inpainting are also used in other render-refine-repeat (RRR) works. These approaches generally tackle the Text-to-3D task and focus exclusively on novel view synthesis. We compare against two SOTA methods LucidDreamer and RealmDreamer (concurrent work), which use a comparable StableDiffusion model as us, and extract the geometry of the scene. For fairness, we test images from their papers and from Waymo, as seen in Fig. 1. There are two main differences: **1)** Due to the focus on NVS, the resulting geometry is subpar, even for

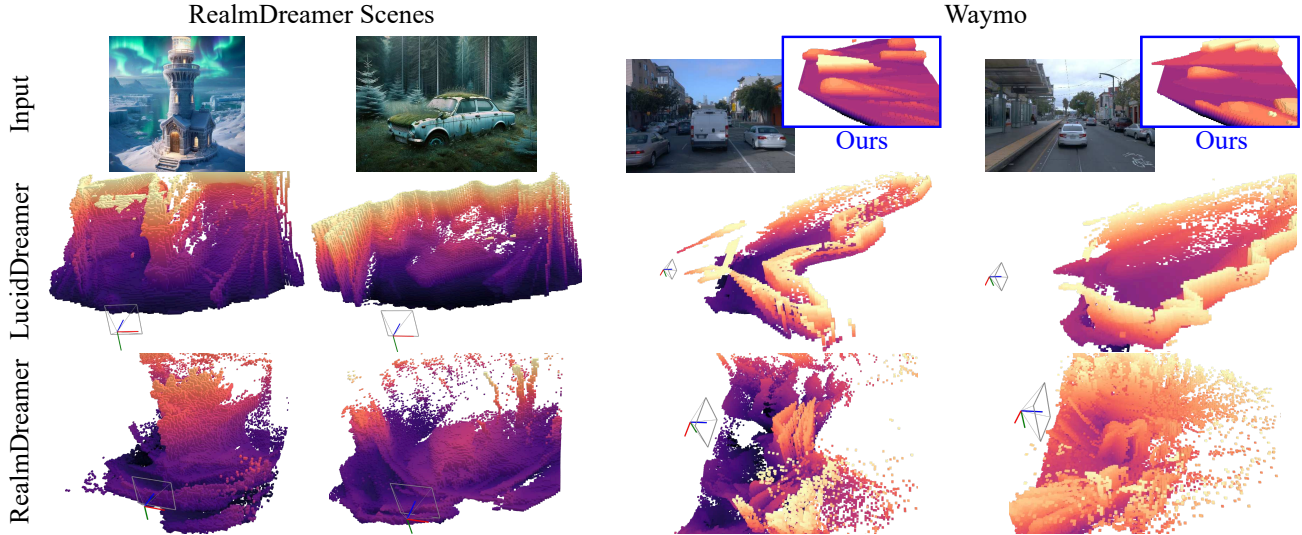


Figure 1. **Render-refine-repeat Comparison.** Occupancy reconstruction for different RRR methods against ours (marked blue).

Depth gradients	Optical flow	PSNR $\uparrow$	Abs Rel $\downarrow$	RMSE $\downarrow$
$\checkmark$	$\times$	<b>20.920</b>	<b>0.133</b>	<b>0.093</b>
$\times$	$\checkmark$	18.707	0.179	0.121
$\checkmark$	$\checkmark$	18.933	0.179	0.118

Table 1. **Qualitative occlusion detection strategies.** Strategies during inference in the novel view. at  $192 \times 640$  resolution

example images from their papers. Here, our *synthetic occupancy field* comes into play. **2)** Because of the focus on Text-to-3D rather than Image-to-3D, existing RRR methods work well for images generated using the diffusion model itself (often in cartoon or fantasy-style). Here, the diffusion model can inpaint effectively even without finetuning. However, when using real images, the inpainting produces poor results. Our novel *VCM* with the corresponding warp-based training solves this issue.

## D. Additional Experiments

**Quantitative effect of occlusions.** We measure the effect of the occlusion maps for different methods also quantitatively in Tab. 1. As observed in the main paper, the depth gradient-based approach performs best.

**Effect of Warp Distance and Occlusion Strategy on VCM.** As seen in Fig. 2, our gradient-based occlusion detection strategy provides more precise masks ( $\rightarrow$  more visual context) than the flow-based baseline. Thus, the VCM produces better synthetic views. When performing larger

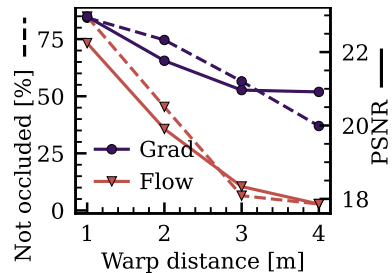


Figure 2. **VCM.** Gradient vs. flow-based occl. detection against warp distance.

viewpoint changes, the quality degrades slightly. In our experiments, novel view poses are on average  $\sim 3$  m away from the source view(s).

**Statistical Importance.** We report the mean and variance where possible in Tab. 2 a). The variance remains within limits, meaning that the final results are reliable.

**Impact of supervision via the SOF.** To test the effect of our geometry synthesis independently of the VCM, we build the synthetic occupancy field directly from real multi-view data (the same as in BTS) and report the results in Tab. 2 b). While the resulting geometry is better than the one produced by BTS, it is still inferior to the geometry resulting from the synthetic views produced by the VCM. This suggests that both the VCM and our novel way of obtaining scene geometry contribute to our strong performance.

**Inference Latency.** While the SOF geometry is of high-

<i>Method</i>	$O_{acc} \uparrow$	$IE_{acc} \uparrow$	$IE_{rec} \uparrow$	$O_{acc} \uparrow$	$IE_{acc} \uparrow$	$IE_{rec} \uparrow$
<i>a)</i> BTS	92 <sub>0.64</sub>	69 <sub>4.24</sub>	64 <sub>8.37</sub>	95 <sub>0.74</sub>	63 <sub>10.71</sub>	94 <sub>1.88</sub>
BTS-D	92 <sub>0.70</sub>	70 <sub>3.96</sub>	66 <sub>8.24</sub>	95 <sub>0.77</sub>	61 <sub>11.66</sub>	96 <sub>1.11</sub>
<b>Ours</b>	93 <sub>0.49</sub>	72 <sub>3.51</sub>	74 <sub>6.67</sub>	97 <sub>0.35</sub>	73 <sub>6.82</sub>	96 <sub>1.35</sub>
<b>Ours (Distilled)</b>	90 <sub>0.86</sub>	71 <sub>3.84</sub>	71 <sub>9.00</sub>	96 <sub>0.43</sub>	72 <sub>7.10</sub>	93 <sub>2.69</sub>
<i>b)</i> <b>Ours</b>	93 <sub>0.49</sub>	72 <sub>3.51</sub>	74 <sub>6.67</sub>	97 <sub>0.35</sub>	73 <sub>6.82</sub>	96 <sub>1.35</sub>
Ours w/ real MV	93 <sub>0.50</sub>	71 <sub>3.91</sub>	66 <sub>7.62</sub>	97 <sub>0.25</sub>	71 <sub>7.07</sub>	91 <sub>3.25</sub>

Table 2. **Scene Reconstruction.** *a)* Results on KITTI-360 / Waymo in % with variances. *b)* Comparing synthesized views vs. real multi-view data for building the synthetic occupancy field.

quality, the generation process is costly at  $5303 \frac{\text{ms}}{\text{frame}}$  on an A100 GPU. The distilled scene reconstruction model only takes about  $75 \frac{\text{ms}}{\text{frame}}$  ( $>70x$  faster) and is real-time capable. It also produces more stable results, while the original synthesized geometry sometimes contains artifacts. Both aspects are crucial for the applications we target (autonomous driving, robotics, etc.).